



PCCP

Oxygen-induced changes to selectivity-determining steps in electrocatalytic CO₂ reduction

| | |
|-------------------------------|---|
| Journal: | <i>Physical Chemistry Chemical Physics</i> |
| Manuscript ID: | CP-ART-08-2014-003783.R1 |
| Article Type: | Paper |
| Date Submitted by the Author: | 16-Dec-2014 |
| Complete List of Authors: | Zhang, Yinjia; Brown University, Department of Chemistry Peterson, Andrew; Brown University, School of Engineering |
| | |

SCHOLARONE™
Manuscripts

Oxygen-induced changes to selectivity-determining steps in electrocatalytic CO₂ reduction

Yin-Jia Zhang¹, Andrew A. Peterson^{2,*}

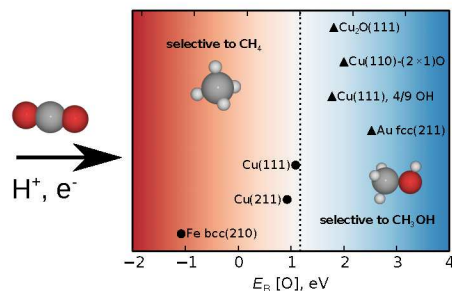
¹*Department of Chemistry and* ²*School of Engineering, Brown University, Providence, Rhode Island, 02912, United States.*

**andrew_peterson@brown.edu*

Abstract

The state of the electrocatalyst surface — including the oxidation state of the catalyst and the presence of spectator species — is investigated on Cu surfaces with density functional theory in order to understand predicted ramifications on the selectivity and efficiency of CO₂ reduction. We examined the presence of oxygen-based species, including the fully oxidized Cu₂O surface, the partially oxidized Cu(110)-(2×1)O surface, and the presence of OH spectators. The relative oxygen binding strength among these surfaces can help to explain the experimentally observed selectivity change between CH₄ and CH₃OH on these electrodes; this suggests that the oxygen-binding strength may be a key parameter which predicts the thermodynamically preferred selectivity for pathways proceeding through a methoxy (CH₃O) intermediate. This study shows the importance of the local surface environment in the product selectivity of electrocatalysis, and suggests a simple descriptor that can aid in the design of improved electrocatalytic materials.

Keywords: coverage, carbon dioxide reduction, selectivity

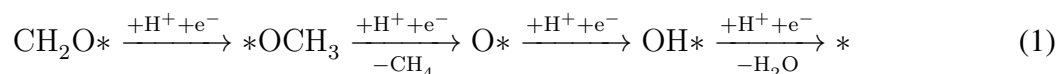


1 Introduction

The externalities associated with carbon dioxide accumulation in the atmosphere, the supply fluctuations of fossil fuels and biofuels, and the anticipated storage demands associated with intermittent electricity sources has sparked a flurry of interest into the conversion of carbon dioxide into fuels and chemicals [1–20]. Electrochemically reducing CO_2 is a promising method to turn this abundant yet undesirable greenhouse gas into useful fuels and chemicals, such as hydrocarbons and alcohols.

Control of product selectivity to liquid fuel products is especially attractive due to the heavy use of liquid fuels in our transportation infrastructure, but our current understanding on the product selectivity mechanism is limited. Recent theoretical studies have focused more on the fundamental reasons of the overpotential requirement, which dictates the energetic efficiency of the process [21–24]. To improve product selectivity is arguably as important and challenging as to lower the overpotential; particularly the selectivity among gas-phase fuels (such as methane and ethane), liquid fuels (such as methanol and ethanol), and chemical precursors (such as ethylene). Some transition metal catalysts show high selectivity towards carbon monoxide or formic acid [2,25,26], but no catalyst has shown an excellent selectivity to liquid fuel products. On pure metallic copper, the most widely studied heterogeneous electrocatalyst for CO_2 reduction, gaseous methane is the dominant product (Faradaic efficiency or FE 40%) with very little liquid fuels, such as methanol [14,27–29]. When changing the operation potentials or the surface roughness and structure of copper electrocatalysts, larger quantities of ethylene [29,30] or formic acid can be generated [18,31].

However, the production of methanol, a liquid product, seems to be preferred in the presence of oxygen on the copper surface. Frese [32] first reported that when the starting copper electrocatalyst material is intentionally oxidized, methanol will be observed while the catalyst surface remains in its oxidized state. Flake and colleagues also reported a preference in CH₃OH generation (FE 38%) on electrodeposited cuprous oxide films [11, 33]. As noted in these papers [32, 33], even though one would not expect long-term stability from these oxide layers on the copper surface under reducing conditions, the oxide layer is speculated to last long enough that the selectivity changes can be attributed to its presence. The existence of oxygen-containing spectator species, such as OH, may also play a similar role as the oxidized surface above. An interesting study by Schouten *et al.* [12] examined the reduction of formaldehyde (CH₂O) and reported that methanol was more preferred than methane when scanning to a more negative potential. Although adsorbed CH₂O has been suggested to be an intermediate in the pathway of CO₂ conversion to CH₄ [21], the potential-limiting step is presumably different when the pathway starts from CH₂O. For CO₂ reduction on transition metals, it is considered that the hydrogenation of adsorbed CO, rather than the activation of CO₂ itself, dictates the overpotential requirement [23]. This difficulty in CO hydrogenation should make it the most abundant spectator during CO₂ reduction. If CH₂O reduction follows the same pathway as suggested for CO₂, the following steps comprise the lowest free-energy change mechanism to methane [21].



However, unlike in CO₂ reduction, the potential-limiting step cannot be the hydrogenation of adsorbed CO, since CO is not present. Instead, the thermodynamic analysis from earlier papers would suggest that the potential-limiting step is the removal of adsorbed hydroxyl species (OH*) [21]. This analysis would suggest the reduction of CH₂O to take place at more positive potentials than that of CO₂, consistent with the measurements of Schouten [12]. With OH removal as the thermodynamically most difficult step, we can expect that OH species are the dominant spectators on this surface. In this work, we will also examine whether spectators such as CO and OH are capable of

changing the predicted selectivity between CH_4 and CH_3OH .

In other areas of catalysis, changes in the selectivity of catalytic reactions have been reported to arise from modifications in the state of the catalyst surface, including surface structure, surface state (*e.g.*, oxidized, reduced, carburized), and the presence of spectator species (often referred to as poisons and promoters). Examples can be found widely, such as the activation of iron oxide catalysts due to carbon deposition in Fischer-Tropsch synthesis of hydrocarbons [34–36], supercritical-water methanation catalysis that activates when RuO_2 is converted to Ru [37, 38], hydrogen evolution activity being poisoned or promoted due to a high coverage of CO spectators [39], changes in the crystalline structure of copper electrodes in CO_2 reduction [40], and many well-known examples of sulfur or carbon monoxide poisoning in methanol oxidation and oxygen reduction materials [41–49].

In the current work, we used density functional theory (DFT) calculations to study how such a local surface environment modification can affect selectivity in electrochemical CO_2 reduction. From a perspective of elementary energetics, we investigated the presence of several likely surface states of copper, including a clean metallic surface, surfaces under various states of oxidation, and surfaces covered with increasing quantities of OH or CO spectators. An analysis of the free energy diagram suggests that the selectivity preference switches to methanol in the cases when copper surface is fully or partially oxidized and when the surface is covered by OH with a high coverage. From this, we suggest a simple activity descriptor as a useful indicator of the selectivity between methane and methanol.

2 Methods

Electronic structure calculations. The Atomic Simulation Environment (ASE) was used to build surface models and DACAPO was employed to conduct DFT calculations [50,51] with the exchange–correlation interactions treated by the RPBE functional [52] and the core electrons treated with Vanderbilt ultrasoft pseudopotentials [53]. The planewave cutoff was set at 340.15 eV and

the density cutoff at 500 eV. Fermi smearing of 0.1 eV and a k -point sampling of $(4 \times 4 \times 1)$ were applied in all surface calculations. A dipole correction was included in the vacuum in the direction orthogonal to the slab surface. The line-search BFGS algorithm was used to relax geometric configurations until the maximum force on any unconstrained atom was less than 0.05 eV/atom. All surfaces were built with 20 Å vacuum between layers and periodic boundary conditions in all directions.

For oxidized copper surfaces, $\text{Cu}_2\text{O}(111)$ and $\text{Cu}(110)-(2 \times 1)\text{O}$ were examined. Cuprous oxide (Cu_2O), has a spacegroup of $Pn-3m$ with the oxygen and copper atoms forming bcc and fcc sublattices, respectively [54, 55]. Experimentally measured lattice constants for cuprous oxide are in the range of 4.268–4.270 Å [56–58]. Our optimized lattice constant is 4.413 Å with k -point sampling of $(4 \times 4 \times 4)$, typical of lattice-constant discrepancies calculated in DFT. A copper terminated surface of Cu_2O (111) was employed. In optimization the top (Cu) layer was relaxed with the subsurface atoms fixed. $\text{Cu}(110)-(2 \times 1)\text{O}$ was built based on $\text{Cu}(110)$ surface by adding a surface oxide layer. Calculations on $\text{Cu}(110)-(2 \times 1)\text{O}$ were carried out with the bottom three layers fixed and the topmost layer relaxed.

For pure copper surfaces covered with spectator species, $\text{Cu}(111)$ covered by OH and CO were investigated and compared. Copper surfaces were cut from an fcc copper bulk crystal with a lattice constant of 3.71 Å, corresponding to the DFT-optimum bulk lattice constant for these electronic-structure parameters [21]. A $3 \times 3 \times 3$ (atoms) periodic cell was employed in our calculations, with the bottom two layers fixed and the top layer relaxed. Herein we focus on the $\text{Cu}(111)$ surface for simplicity in deducing trends, as compared to more highly ordered surfaces such as (211) which may result in coverage patterns unique to the highly periodic system.

Free energy calculations With the electronic potential energies (E_{elec}) obtained from the above DFT calculations, free energies (G) at 25°C were calculated by adding the contributions of zero-point energy (E_{ZPE}), heat capacity (C_p) and entropy, which were all calculated in the harmonic approximation with vibrational energies derived from a normal-mode analysis, as in:

$$G \equiv E_{\text{elec}} + E_{\text{ZPE}} + \int C_p dT - TS \quad (2)$$

where G is our consistently-referenced free energy of a species and T is the temperature.

The normal modes were calculated by a finite-difference approximation of the Hessian matrix with a displacement of 0.01 Å in three dimensions. The vibrational frequencies of each molecule and adsorbate are listed in our Supporting Information. Non-surface-bound species, such as CH₄ and CH₃OH, were treated as independent ideal-gas molecules in a 15×15×15 vacuum box at 101325 Pa. For adsorbates on a surface, the normal modes of an adsorbate were obtained from previous theoretical studies, and taken to be independent of the surface types and any surrounding spectators [21, 22]. Changes in the vibrational contributions to the free energy of lattice and spectator species caused by the presence of our adsorbates were ignored.

The computational hydrogen electrode (CHE) model was applied when calculating the free energy change between two electrochemical steps involving a proton and an electron transfer. This method was proposed by Nørskov *et al.* [59] and its application to CO₂ reduction has been described in detail in previous work [21].

Coverage-dependent binding energies. The task of finding the lowest-energy configuration in high-coverage scenarios is complicated by the combinatorics: there can be hundreds or even thousands of possible configurations [60]. We used a two-part strategy to search for these configurations. First, to evaluate the OH and CO coverage effects on the binding energy of O and CH₃O, a “brute-force” optimization method was used to search for the lowest energy spectator configurations with O and CH₃O at their preferred binding sites, similar to our approach in a previous work [39]. First, O (or CH₃O) was allowed to bind to the (111) surface at all conceivable sites, and the structures were optimized. It was found that a three-fold fcc site is preferred by both adsorbates, consistent with previous studies [22, 61]. Then, with the O (or CH₃O) at its preferred site, a multitude of surfaces were set up with one O (or CH₃O) and x OH (or CO) molecules at various sites on the (111) surface, for $x=1, 2, 3, 4$. These surfaces with O (or CH₃O) and OH (or

CO) groups were relaxed and their potential energies were obtained. For each set of x spectators with a particular adsorbate, the lowest energy configuration was selected, and its potential energy is denoted, for example, as $E[\text{O} + x\text{OH} + *]$. By removing O (or CH_3O) from the lowest energy surface, we optimized the structure again and denote its potential energy without O (or CH_3O) as, for example, $E[x\text{OH} + *]$. From these data, the binding energies of O (or CH_3O) on surfaces with different spectator species presented were defined as, for example

$$E_{\text{B}}[\text{O}; x\text{OH}] \equiv E[\text{O} + x\text{OH} + *] - (E[x\text{OH} + *] + E_{\text{ref}}[\text{O}]) \quad (3)$$

where CH_3O can replace O and CO can replace OH. The arbitrary reference energies were taken as

$$E_{\text{ref}}[\text{O}] = E[\text{H}_2\text{O}] - E[\text{H}_2]$$

$$E_{\text{ref}}[\text{CH}_3\text{O}] = E[\text{CH}_3\text{OH}] - \frac{1}{2}E[\text{H}_2]$$

Coverages are reported in fraction of a monolayer (ML); a monolayer is defined as one adsorbate molecule per surface catalyst atom – that is, a $2/9$ ML coverage of OH corresponds to 2 hydroxyl groups on a periodic 3×3 copper surface.

Simultaneously, a constrained minima-hopping algorithm [60] was applied in order to search for the global lowest energy of each configuration. The results are used to compare with those found by brute-force optimization. Both approaches revealed the identical conformer as the global optimum. By the two-part method, there is a reasonable degree of certainty that the configurations and energies reported correspond to global optima within these constraints.

3 Results and discussion

Oxidized copper surface. In order to assess effects from oxidized copper surfaces, we examined both a bulk oxide and a surface oxide of copper. For the fully oxidized bulk structure, we examined

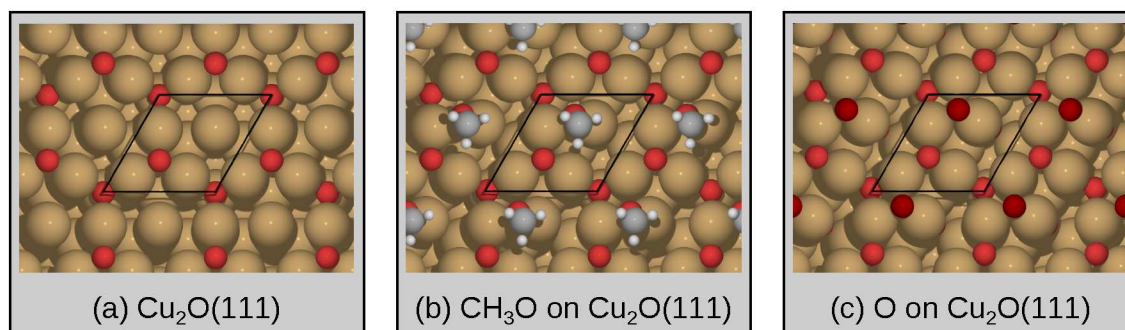


Figure 1: Top view of geometric configurations (a) without and with (b) CH_3O or (c) O adsorbates on the bulk oxide terminated at the $\text{Cu}_2\text{O}(111)$ surface. Color scheme: C gray, O red, H white, Cu copper. The periodic unit cell is shown in black lines.

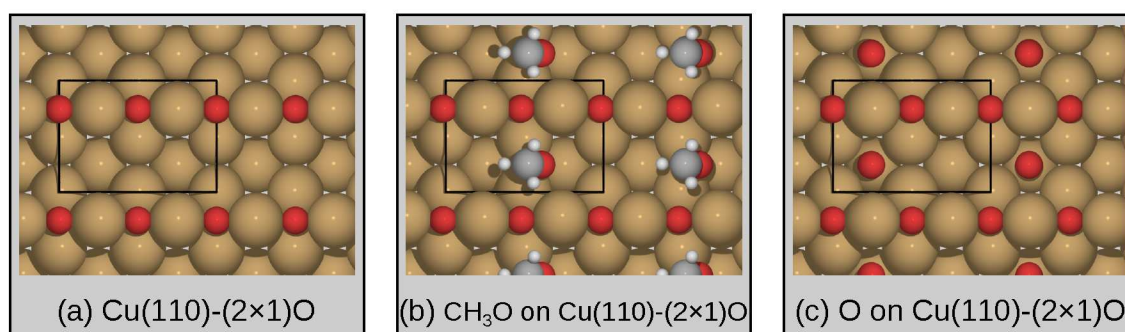


Figure 2: Top view of geometric configurations (a) without and with (b) CH_3O or (c) O adsorbates on the surface oxide represented by $\text{Cu}(110)-(2\times 1)\text{O}$. Color scheme: C gray, O red, H white, Cu copper. The periodic unit cell is shown in black lines.

cuprous oxide (Cu_2O), which is one of the principle oxides of copper and has been reported to reduce CO_2 to CH_3OH [11, 33, 62]. For the partially oxidized copper surface, we studied $\text{Cu}(110)-(2\times 1)\text{O}$. This structure was shown to be formed with oxygen molecules dissociatively adsorbed on a copper surface at room temperature [63]. Although it is not known if the continued production of oxygen adsorbates on a copper surface could lead to such a structure in the electrochemical environment, this system nevertheless provides a reasonable model system in the spectrum of copper surfaces with different levels of oxidation.

On the $\text{Cu}_2\text{O}(111)$ surface both CH_3O and O favor the fcc three-fold site as shown in Figure 1. On $\text{Cu}(110)-(2\times 1)\text{O}$, both CH_3O and O tend to bind between top copper atom rows: CH_3O stays near the bridge site and O locates in the center of the four-fold site (Figure 2). The electronic potential energy calculations provide the basis for the elementary thermodynamic free energy di-

agrams in the CHE model, shown in Figure 3. The results are also compared with the free energy diagram of a non-oxidized Cu(111) surface. On the pure Cu(111) surface, the hydrogenation of adsorbed CH_3O thermodynamically favors the generation of methane, which is 0.2 eV lower than the free-energy change for methanol generation. This is consistent with previous theoretical studies [22] and experimental observations of CH_4 formation on Cu(111) surfaces [64]. However, the thermodynamics are reversed on oxidized copper surfaces. On both $\text{Cu}_2\text{O}(111)$ and $\text{Cu}(110)-(2\times 1)\text{O}$, the free energy of $(\text{CH}_3\text{OH} + *)$ is 0.6-0.7 eV lower than that of $(\text{CH}_4 + \text{O}^*)$, suggesting that methanol is thermodynamically preferred by this pathway on oxidized copper electrocatalysts. These changes are directly related to the weakening of the surface-oxygen bond. This is consistent with the before-mentioned experimental observations of direct CO_2 to CH_3OH electrochemical reduction in aqueous solutions, which has been reported on intentionally oxidized copper surfaces [11,33,62].

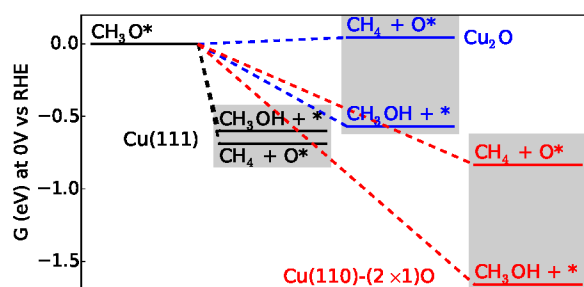


Figure 3: Free energy diagram of the electrochemical step from CH_3O on Cu(111), $\text{Cu}_2\text{O}(111)$ and $\text{Cu}(110)-(2\times 1)\text{O}$. All data are plotted relative to the free energy of CH_3O^* for each surface. The step involves transfer of a proton and electron ($\text{H}^+ + \text{e}^-$) in the CHE model calculated at 0 V vs RHE.

Co-adsorbed spectators on copper surface. To study the effect of co-adsorbed OH on the thermodynamically predicted pathways, we examined surfaces covered with increasing coverages of OH or CO spectators. We chose a surface covered in OH in order to understand the conditions that may result from a partially oxidized surface or in which OH removal is the limiting step, as it may be in formaldehyde reduction. We compare the energetics to those of a bare copper surface; however, a fairer comparison may be to CO-covered surfaces, as we would expect a high CO coverage

if CO hydrogenation is the most difficult step. Thus, we also include CO-covered surfaces in our analysis.

We first describe the geometric configurations of OH on Cu, which shows that OH tends to self-stabilize moderate coverages by setting up a hydrogen-bonding network. Figure 4 shows the geometric configurations of CH₃O and O with spectators OH or CO on a Cu(111) surface; both CH₃O and O are maintained at their preferred three-fold fcc sites in all cases. CH₃O binds to copper through its oxygen atom and the methyl group points away from the surface. Like the oxygen atom and the methoxy group, the OH spectators also tend to favor three-fold sites at most coverage levels. When OH is at 1/9 ML coverage, the O–H bond tends to be vertical to the surface. As the coverage of OH increases, a hydrogen bonding network starts to be established and the orientation of the O–H bond in OH starts to parallel the surface. Note that on surfaces with O adsorbed, some O–H bonds stay vertically oriented even when the OH coverage is 2/9 or 3/9 ML; while this does not occur on the surfaces with CH₃O. This may be caused by the larger size of CH₃O relative to O and a repulsion between hydrogen atoms in OH and CH₃O.

The behavior of carbon monoxide (CO) spectators is different from hydroxyl, primarily because CO adsorbates tend to repel one another [65–68], as opposed to the attraction in hydrogen binding networks. CO binds to copper through a carbon atom, and tends to favor both ontop sites and three-fold sites. Adsorbate-adsorbate hydrogen bonding does not exist in this case and the interaction between carbon in CO and oxygen in CH₃O or O is much weaker than that between hydrogen and oxygen. Thus, CO prefers to be oriented away from the copper surface even when its coverage is high. This weak interaction makes CO spectators tend to distribute rather uniformly on a surface. It is also noted that the distance between CO and O is smaller than that between CO and CH₃O, which can also be attributed to the size difference between CH₃O and O.

The corresponding binding energy calculation results are summarized in Figure 6. For surfaces with spectators of OH, these calculations suggest that a high coverage of OH weakens the binding of both CH₃O and O. As the coverage of OH increases from zero to 2/9 ML, the binding energy becomes slightly stronger, by less than 0.1 eV. At 3/9 ML coverage, OH spectators can build a

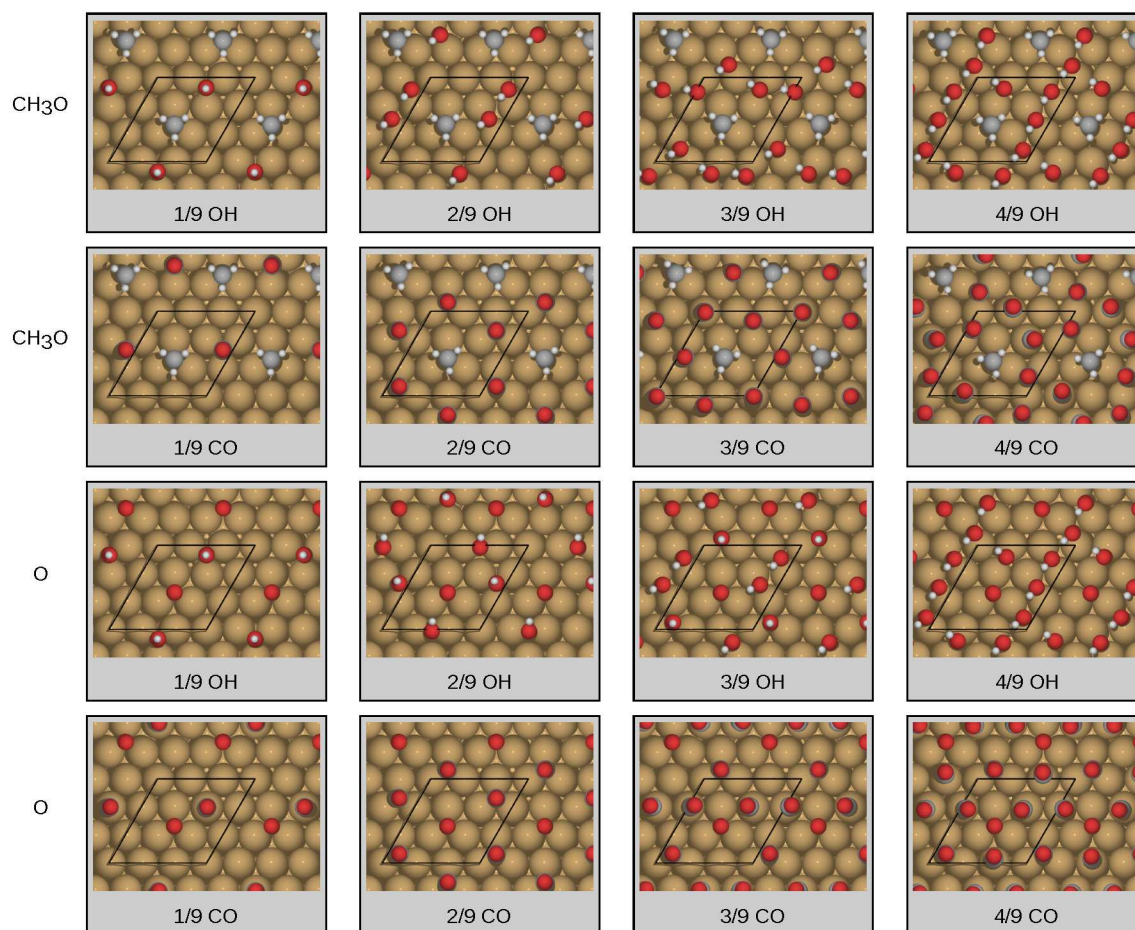


Figure 4: Top view of the geometric configurations of the Cu(111) surface with adsorbates CH_3O or O and spectators OH or CO . Color scheme: C gray, O red, H white, Cu copper. The periodic unit cell is shown in black lines.

strong hydrogen bonding network even if CH_3O or O is not on surface. As shown in Figure 5, a line of OH is formed within these geometric constraints. The addition of a CH_3O or O will not only destroy the tight network, but increase the repulsion between molecules as well, causing the binding energy to increase sharply at $4/9$ ML of OH . In practice, we would expect the presence of liquid water to make this effect more pronounced.

Similarly, a higher coverage of CO will lead to a weaker binding energy of methoxy CH_3O . This trend is consistent with previous studies on the CHO binding strength change with CO coverage on a Pt surface [69]. At low coverages of $1/9$ ML and $2/9$ ML CO , the interactions are weak and the binding energy changes of both CH_3O and O are within typical accuracies of DFT. When CO accumulates on the surface, the binding energy of CH_3O increases rapidly due to a forced

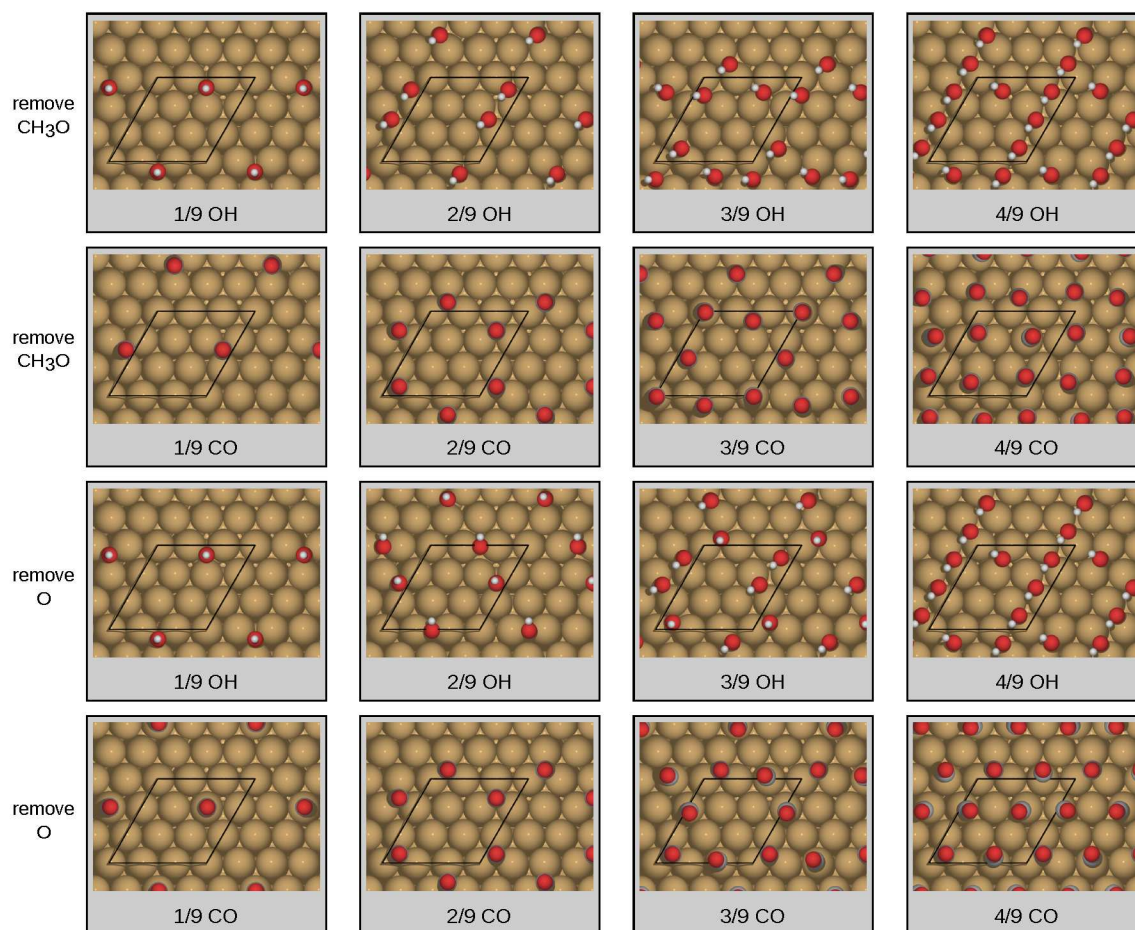


Figure 5: Top view of the geometric configurations of Cu(111) surface when adsorbate CH_3O or O is removed. Color scheme: C gray, O red, H white, Cu copper. The periodic unit cell is shown in black lines.

change in CO binding sites. For example, at $4/9$ ML, with CH_3O on the surface CO molecules occupy two ontop sites and two threefold sites. However, after removing CH_3O and re-optimizing the structure, one of the ontop CO adsorbates drifts to a nearby bridge site, effectively trying to adopt a uniform spacing on the surface. These steric effects on CO account for most of the incremental binding energy; this can be observed as the geometric effects in the binding energy shown in Figure 6(b). As a smaller adsorbate, an oxygen atom apparently has a much smaller steric effect on the CO distribution. This is readily apparent in Figure 6(d), in which a geometric effect is essentially absent, and can also be seen geometrically in the $4/9$ ML CO configurations in Figure 4. In these figures, the methoxy group has a larger CO-free zone surrounding it than does the oxygen. Although there are some ups and downs in the O binding energy when changing the CO coverage,

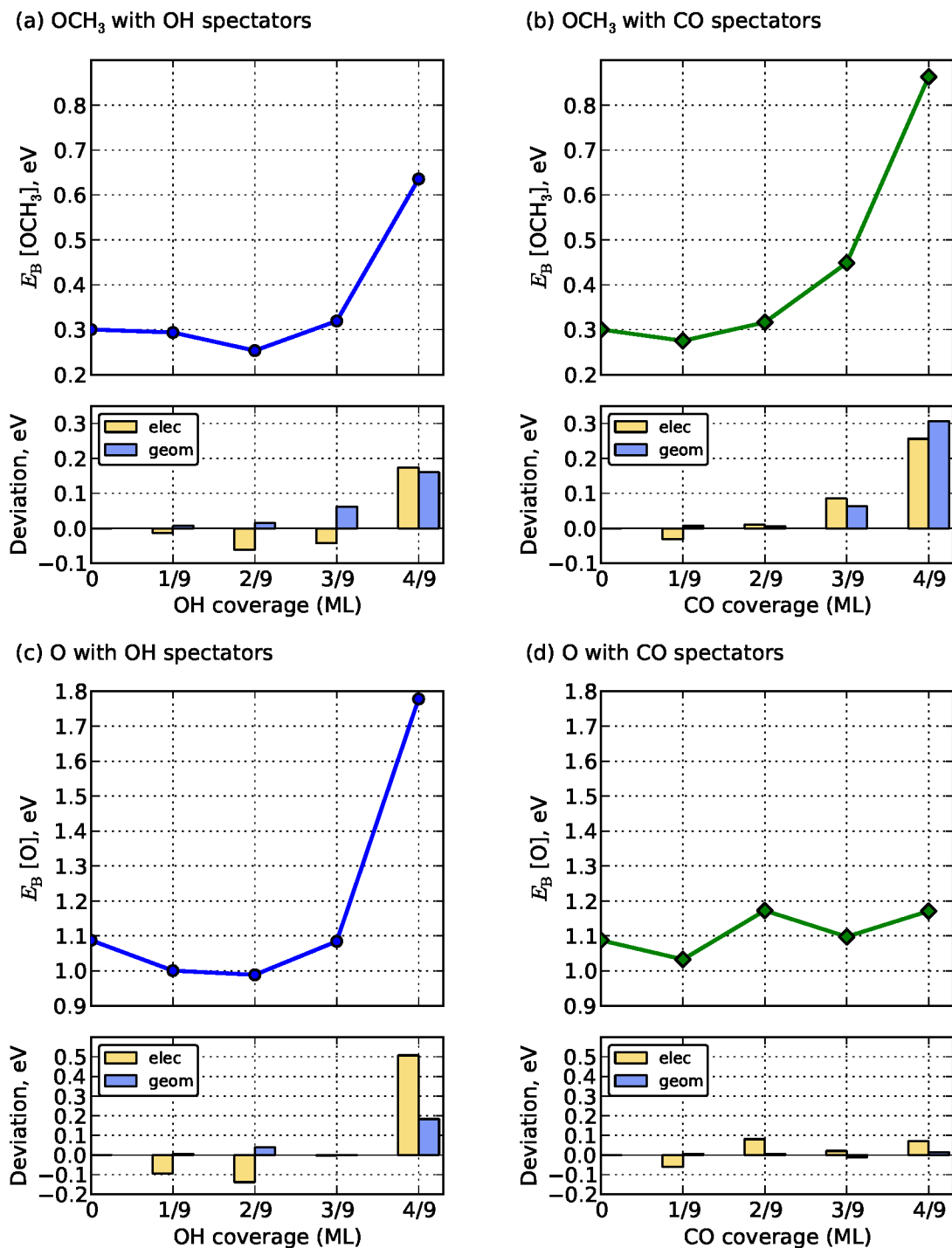


Figure 6: Binding energy of CH_3O and O vs the coverage, of OH or CO on $\text{Cu}(111)$ surface. In the lower figures, the deviation of the energy from that in the absence of spectators is broken down into electronic ('elec') and geometric ('geom') effects, which sum to the difference between the binding energy at the specified spectator coverage and the binding energy without spectators. The electronic effect is the difference in binding energy when the adsorbate is removed without allowing the spectators to re-arrange; the geometric effect is the binding energy difference upon allowing for re-arrangement of the spectator species and the top surface layer.

they occur in a limited range (± 0.1 eV), suggesting that CO doesn't have a significant effect on O binding energy at these coverages. This is in contrast to the results at high OH coverages.

OH/CO coverage effects on product selectivity. To understand the effects on the binding energy in the context of the elementary reduction of $*\text{OCH}_3$ to $(\text{CH}_3\text{OH} + *)$ or $(\text{CH}_4 + *)$, Figure 7 shows a free energy diagram of this elementary step which can determine the selectivity to the final carbon-containing product, either CH_4 or CH_3OH . In agreement with earlier studies [22], on a clean Cu(111) surface the liberation of CH_4 is more favorable than the liberation of CH_3OH , suggesting a thermodynamic selectivity towards CH_4 . The blue and green lines indicate the revised potential energies by including the effect of OH and CO spectators on the Cu(111) surface. When CO_2/CO is reduced, the main spectator on the surface is CO. As seen in Figure 7, the energy changes associated with CO coverage still point towards a weak-to-neutral selectivity preference of CH_4 over CH_3OH , suggesting that the high CO coverages that would be expected to be present in CO_2/CO reduction do not qualitatively change the selectivity of a clean surface. On the other hand, as the coverage of OH spectators increases, the energy of $(\text{CH}_4 + \text{O}^*)$ becomes up to ~ 0.5 eV higher than that of $(\text{CH}_3\text{OH} + *)$. Therefore, as the OH coverage increases, CH_3OH becomes thermodynamically more favorable at this step. This indicates that OH coverage is thermodynamically more than strong enough to flip the selectivity, while CO coverage is not.

The above changes due to the surface coverage conditions may give us some insights on the time-based changes observed in Schouten and Koper's work. While the equilibrated existence of methanediol (in addition to formaldehyde) in aqueous solutions may explain much of the methanol production under these conditions [70], it is possible that oxygen-induced changes to the catalyst surface are responsible for the selectivity change observed from methane to methanol over the course of Schouten's reductive sweep. In the OLEMS (online electrochemical mass spectroscopy) spectra of formaldehyde reduction reported in their work (Figure 3 in reference [12], the $m/z = 15$ curve (fragments from CH_4) separates from the $m/z = 29, 30, 31$ curves (fragments from CH_3OH) in the sweep region from -0.3 to -0.55 V vs RHE. The experiment is carried out by changing the

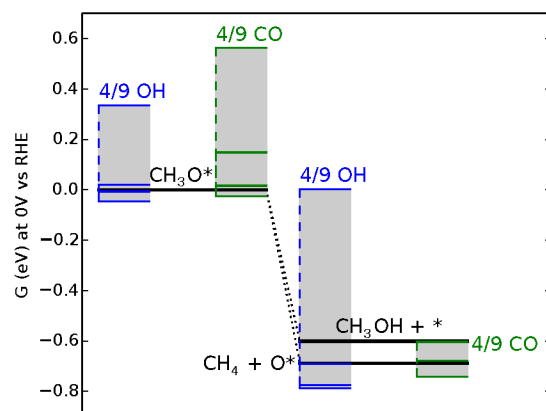


Figure 7: Cu(111) surface coverage-dependent free energy diagram. Black lines are potential energies obtained on bare surface with no OH or CO spectator species; blue lines represent OH adsorbed; green lines represent CO adsorbed.

potential of the electrode from 0.0 to -1.0 V and back at $1 \text{ mV} \cdot \text{s}^{-1}$. Although the OLEMS data do not quantify the amounts of CH_4 and CH_3OH produced in these experiments, they suggest a change in selectivity from $\text{CH}_4 + \text{CH}_3\text{OH}$ (early times) to predominantly CH_3OH (later times). On the reverse sweep, the change in selectivity is not observed, suggesting that the selectivity changes correlate with time more strongly than potential. The simplest explanation for a time-based change from methane to methanol could be a change in the catalyst condition. Initially, the bare surface would have selectivity predominantly to methane (Figure 7). As hydroxyl groups gradually build up and form a network during formaldehyde reduction, the free energy of $(\text{CH}_4 + \text{O}^*)$ increases and finally exceeds that of $(\text{CH}_3\text{OH} + *)$. Thus the main product changes to CH_3OH . Once the surface is sufficiently coated in OH spectators, it only takes a small amount of the methane-forming reaction occurring in parallel with the methanol-forming reaction in order to keep the surface coated in these species, and keep the selectivity predominantly towards methanol.

Although a full coverage-dependent kinetic Monte Carlo model in the presence of explicit water molecules might be necessary to make quantitative predictions on the potential-dependent reactive coverage of OH and CO species in the different reactive systems (CO_2 reduction and CH_2O reduction), we can use the trends in binding energies to make some qualitative conclusions

regarding coverages of OH and CO under reactive conditions. At CO₂/CO experimental reaction conditions (-0.8 to -1.0 V vs RHE to generate CH₄ primarily), the reactive conversion of CO to CHO is the most difficult step from an elementary thermodynamics standpoint and is just exergonic; similarly, at the CH₂O reduction conditions (-0.4 to -0.7 V vs RHE to generate CH₃OH and/or CH₄) the removal of OH is the most difficult step and is also just exergonic, by roughly the same value. Therefore, the inference of a reasonable OH coverage under CH₂O-reducing conditions is equivalent, on the basis of these calculations, to the inference of a reasonable CO coverage under CO₂/CO-reducing conditions. We can use the relative binding energies of these species as a function of coverage to give us an indication of the relative reactive coverages expected. We know that CO adsorbates tend to repel each other [65–68], suggesting that a lower equilibrium coverage may be favorable, whereas OH adsorbates tend to stabilize each other through a hydrogen-bonding network [71–73] suggesting that under these comparable overpotential conditions, we should expect the coverage of OH under formaldehyde-reducing conditions to be at least as high as the coverage of CO under CO₂ reducing conditions, if not higher. Water will also participate in the hydrogen-bonding network, further stabilizing hydroxyl species on the surface [74].

Selectivity descriptor. By examining the information above, it is apparent that the thermodynamically favored product of methoxy reduction is only related to the binding energy of oxygen on the surface. We therefore suggest that the oxygen binding energy of the active catalyst surface can be used as a first-order descriptor of the selectivity towards methane or methanol, at least among pathways that proceed through a methoxy intermediate. The data in the current article are summarized in Figure 8, which shows the oxygen binding energy along with the theoretically predicted selectivity based on our calculations. Pure copper facets sit below the cutoff binding energy of ~ 1.17 eV (dashed line) and prefer methane in CO₂ or CO reduction; while oxidized and hydroxyl covered copper surfaces are above the cutoff line and prefer methanol as a reducing product. This is consistent with the experimentally observed trends. Interestingly, Kuhl and co-workers [76] performed CO₂ reduction with high product selectivity on a range of electrocatalytic materials

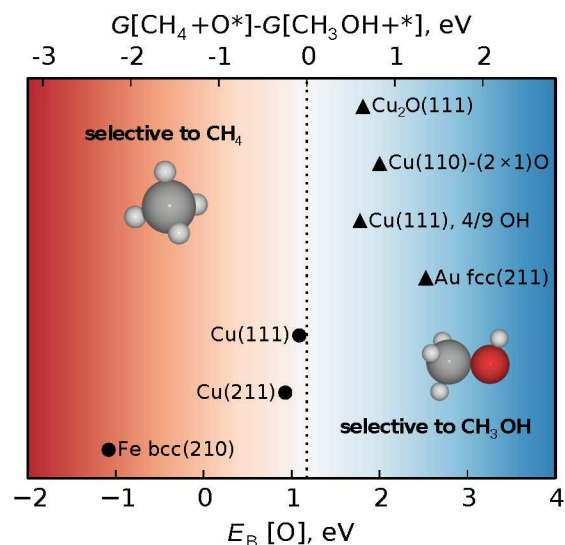


Figure 8: Oxygen binding energy as an activity descriptor for $\text{CH}_4/\text{CH}_3\text{OH}$ selectivity. Circle (●): selective to CH_4 ; Triangle (▲): selective to CH_3OH . The dashed-line indicates the cutoff binding energy at which the thermodynamic selectivity of the elementary step changes between methane and methanol. Some $E_B[\text{O}]$ values come from literature: $\text{Cu}(211)$ [21], $\text{Fe bcc}(210)$ [75] and $\text{Au fcc}(211)$ [75]. Experimental product observations have been reported by the following literature: reduced copper [2], copper oxides [32, 33], Fe [76] and Au [76].

and observed products more reduced than CO on a number of materials. Two of these materials showed a strong selectivity preference towards either methane or methanol (Fe and Au); we have added these data points to Figure 8 as well and they are consistent with the descriptor. We note that many other factors, such as pathway changes and elementary barriers, will also influence the selectivity; nonetheless, the simple descriptor of oxygen binding energy here adequately describes the experimentally-observed selectivities among the electrocatalysts examined.

4 Conclusions

The results of these calculations suggest that the thermodynamically predicted pathways in CO_2 reduction can be affected by the local surface environment of the electrocatalyst, particularly by the state of oxidation of copper surfaces. Specifically, the intermediate CH_3O^* can lead to CH_4 or CH_3OH depending on whether the surface is a clean copper surface or one in which a surface or

bulk oxide is present, or on whether OH or CO is the predominant spectator. A moderate amount of oxygen, manifested as oxide formations or hydroxyl spectator groups, has this effect by significantly increasing the electronic energy of ($\text{CH}_4 + \text{O}^*$), leaving CH_3OH as the thermodynamically preferred product under these conditions. This work, along with that by others [12,69], highlights that the local surface environment of a catalyst surface can have a profound impact on the selectivity of elementary reaction steps. This suggests the importance of studying spectator coverage effects on the other crucial steps in CO_2 reduction, such as the initial activation of CO_2 or the hydrogenation of adsorbed CO, and suggests that such surface effects may cause deviations from the scaling effects that are thought to limit the efficiency of CO_2 reduction. In further studies, calculations can be expanded to other possible spectators, such as carbon, which may also affect both Faradaic efficiency and the product selectivity in CO_2 reduction [77]. Finally, an activity descriptor – the binding energy of oxygen to the catalyst surface – has been introduced which is expected to be useful in designing catalysts that selectively produce methanol versus methane from adsorbed methoxy in electrochemical reductions.

ASSOCIATED CONTENT

Supporting Information is available at the publisher's website free of charge. This includes the free energy corrections, coverage-dependent energies, and calculated vibrational modes.

AUTHOR INFORMATION

Corresponding author. *Email: andrew_peterson@brown.edu. Telephone +1 401-863-2153.

Acknowledgments. We gratefully acknowledge financial support from the Young Investigator Award from the Office of Naval Research under award N00014-12-1-0851. Calculations were undertaken at the Center for Computation & Visualization (CCV), Brown University.

References

- [1] M. Gattrell, N. Gupta, and A. Co. A review of the aqueous electrochemical reduction of CO₂ to hydrocarbons at copper. *Journal of Electroanalytical Chemistry*, 594(1):1–19, 2006.
- [2] Y. Hori. Electrochemical CO₂ reduction on metal electrodes. In Constantinos G. Vayenas, Ralph E. White, and Maria E. Gamboa-Aldeco, editors, *Modern Aspects of Electrochemistry*, volume 42 of *Modern Aspects of Electrochemistry*, pages 89–189. Springer New York, 2008.
- [3] Jean-Michel Savéant. Molecular catalysis of electrochemical reactions. Mechanistic aspects. *Chemical Reviews*, 108(7):2348–2378, 2008.
- [4] Charles Delacourt, Paul L. Ridgway, John B. Kerr, and John Newman. Design of an electrochemical cell making syngas (CO + H₂) from CO₂ and H₂O reduction at room temperature. *Journal of the Electrochemical Society*, 155(1):B42–B49, 2008.
- [5] Eric E. Benson, Clifford P. Kubiak, Aaron J. Sathrum, and Jonathan M. Smieja. Electrocatalytic and homogeneous approaches to conversion of CO₂ to liquid fuels. *Chemical Society Reviews*, 38:89–99, 2009.
- [6] M. Rakowski Dubois and Daniel L. Dubois. Development of molecular electrocatalysts for CO₂ reduction and H₂ production/oxidation. *Accounts of Chemical Research*, 42(12):1974–1982, 2009.
- [7] Somnath C. Roy, Oomman K. Varghese, Maggie Paulose, and Craig A. Grimes. Toward solar fuels: Photocatalytic conversion of carbon dioxide to hydrocarbons. *ACS Nano*, 4(3):1259–1278, 2010.
- [8] Donald J. Darensbourg. Chemistry of carbon dioxide relevant to its utilization: A personal perspective. *Inorganic Chemistry*, 49(23):10765–10780, 2010.
- [9] Emily Barton Cole, Prasad S. Lakkaraju, David M. Rampulla, Amanda J. Morris, Esta Abelev, and Andrew B. Bocarsly. Using a one-electron shuttle for the multielectron reduction

- of CO₂ to methanol: Kinetic, mechanistic, and structural insights. *Journal of the American Chemical Society*, 132(33):11539–11551, 2010.
- [10] Devin T. Whipple and Paul J. A. Kenis. Prospects of CO₂ utilization via direct heterogeneous electrochemical reduction. *The Journal of Physical Chemistry Letters*, 1(0):3451–3458, 2010.
- [11] M. Le, M. Ren, Z. Zhang, P. T. Sprunger, R. L. Kurtz, and J. C. Flake. Electrochemical reduction of CO₂ to CH₃OH at copper oxide surfaces. *Journal of The Electrochemical Society*, 158(5):E45–E49, 2011.
- [12] K. J. P. Schouten, Y. Kwon, C. J. M. van der Ham, Z. Qin, and M. T. M. Koper. A new mechanism for the selectivity to C1 and C2 species in the electrochemical reduction of carbon dioxide on copper electrodes. *Chemical Science*, 2:1902–1909, 2011.
- [13] Brian A. Rosen, Amin Salehi-Khojin, Michael R. Thorson, Wei Zhu, Devin T. Whipple, Paul J. A. Kenis, and Richard I. Masel. Ionic liquid–mediated selective conversion of CO₂ to CO at low overpotentials. *Science*, 334(6056):643–644, 2011.
- [14] Kendra P. Kuhl, Etosha R. Cave, David N. Abram, and Thomas F. Jaramillo. New insights into the electrochemical reduction of carbon dioxide on metallic copper surfaces. *Energy Environmental Science*, 5:7050–7059, 2012.
- [15] Zhichuan Xu, Erica Lai, Yang Shao-Horn, and Kimberly Hamad-Schifferli. Compositional dependence of the stability of AuCu alloy nanoparticles. *Chemical Communications*, 48:5626–5628, 2012.
- [16] Douglas R. Kauffman, Dominic Alfonso, Christopher Matranga, Huifeng Qian, and Rongchao Jin. Experimental and computational investigation of Au₂₅ clusters and CO₂: A unique interaction and enhanced electrocatalytic activity. *Journal of the American Chemical Society*, 134(24):10237–10243, 2012.

- [17] Thomas J. LaTempa, Sanju Rani, Ningzhong Bao, and Craig A. Grimes. Generation of fuel from CO₂ saturated liquids using a p-Si nanowire || n-TiO₂ nanotube array photoelectrochemical cell. *Nanoscale*, 4:2245–2250, 2012.
- [18] Christina W. Li and Matthew W. Kanan. CO₂ reduction at low overpotential on Cu electrodes resulting from the reduction of thick Cu₂O films. *Journal of the American Chemical Society*, 134(17):7231–7234, 2012.
- [19] Michael R. Thorson, Karl I. Siil, and Paul J. A. Kenis. Effect of cations on the electrochemical conversion of CO₂ to CO. *Journal of The Electrochemical Society*, 160(1):F69–F74, 2013.
- [20] John A. Keith and Emily A. Carter. Electrochemical reactivities of pyridinium in solution: Consequences for CO₂ reduction mechanisms. *Chemical Science*, 4:1490–1496, 2013.
- [21] Andrew A. Peterson, Frank Abild-Pedersen, Felix Studt, Jan Rossmeisl, and Jens K. Nørskov. How copper catalyzes the electroreduction of carbon dioxide into hydrocarbon fuels. *Energy Environmental Science*, 3:1311–1315, 2010.
- [22] William J. Durand, Andrew A. Peterson, Felix Studt, Frank Abild-Pedersen, and Jens K. Nørskov. Structure effects on the energetics of the electrochemical reduction of CO₂ by copper surfaces. *Surface Science*, 605(15-16):1354–1359, 2011.
- [23] Andrew A. Peterson and Jens K. Nørskov. Activity descriptors for CO₂ electroreduction to methane on transition-metal catalysts. *The Journal of Physical Chemistry Letters*, 3(2):251–258, 2012.
- [24] Xiaowa Nie, Monica R. Esopi, Michael J. Janik, and Aravind Asthagiri. Selectivity of CO₂ reduction on copper electrodes: The role of the kinetics of elementary steps. *Angewandte Chemie International Edition*, 52(9):2459–2462, 2013.
- [25] Wenlei Zhu, Ronald Michalsky, Önder Metin, Haifeng Lv, Shaojun Guo, Christopher J. Wright, Xiaolian Sun, Andrew A. Peterson, and Shouheng Sun. Monodisperse Au nanoparti-

- cles for selective electrocatalytic reduction of CO₂ to CO. *Journal of the American Chemical Society*, 135(45):16833–16836, 2013.
- [26] Wenlei Zhu, Yin-Jia Zhang, Hongyi Zhang, Haifeng Lv, Qing Li, Ronald Michalsky, Andrew A Peterson, and Shouheng Sun. Active and selective conversion of CO₂ to CO on ultrathin Au nanowires. *Journal of the American Chemical Society*, 2014.
- [27] Y. Hori, K. Kikuchi, and S. Suzuki. Production of CO and CH₄ in electrochemical reduction of CO₂ at metal electrodes in aqueous hydrogencarbonate solution. *Chemistry Letters*, 14(11):1695–1698, 1985.
- [28] Y. Hori, K. Kikuchi, A. Murata, and S. Suzuki. Production of methane and ethylene in electrochemical reduction of carbon dioxide at copper electrode in aqueous hydrogencarbonate solution. *Chemistry Letters*, 15(6):897–898, 1986.
- [29] Yoshio Hori, Akira Murata, and Ryutaro Takahashi. Formation of hydrocarbons in the electrochemical reduction of carbon dioxide at a copper electrode in aqueous solution. *Journal of the Chemical Society, Faraday Transactions 1*, 85:2309–2326, 1989.
- [30] Wei Tang, Andrew A. Peterson, Ana Sofia Varela, Zarko P. Jovanov, Lone Bech, William J. Durand, Soren Dahl, Jens K. Nørskov, and Ib Chorkendorff. The importance of surface morphology in controlling the selectivity of polycrystalline copper for CO₂ electroreduction. *Physical Chemistry Chemical Physics*, 14:76–81, 2012.
- [31] Sujat Sen, Dan Liu, and G Tayhas R Palmore. Electrochemical reduction of CO₂ at copper nanofoams. *ACS Catalysis*, 4:3091–3095, 2014.
- [32] Karl W. Frese. Electrochemical reduction of CO₂ at intentionally oxidized copper electrodes. *Journal of The Electrochemical Society*, 138(11):3338–3344, 1991.

- [33] Maoming Ren, Minh Le, Ziyu Zhang, Phillip T. Sprunger, and J. C. Flake. Regenerative methanol fuel cells: Reduction of CO₂ to methanol on oxidized Cu electrodes. *ECS Transactions*, 33(39):253–259, 2011.
- [34] Hans Schulz. Short history and present trends of Fischer-Tropsch synthesis. *Applied Catalysis A: General*, 186(1-2):3 – 12, 1999.
- [35] Jose Gracia, Frans Prinsloo, and J. Niemantsverdriet. Mars-van Krevelen-like mechanism of CO hydrogenation on an iron carbide surface. *Catalysis Letters*, 133:257–261, 2009.
- [36] G.B. Raupp and W.N. Delgass. Mössbauer investigation of supported Fe and FeNi catalysts: II. Carbides formed Fischer-Tropsch synthesis. *Journal of Catalysis*, 58(3):348–360, 1979.
- [37] Andrew A. Peterson, Marian Dreher, Jörg Wambach, Maarten Nachtegaal, Søren Dahl, Jens K. Nørskov, and Frédéric Vogel. Evidence of scrambling over ruthenium-based catalysts in supercritical-water gasification. *ChemCatChem*, 4(8):1185–1189, 2012.
- [38] Marian Dreher, Benjamin Johnson, Andrew A. Peterson, Maarten Nachtegaal, Jörg Wambach, and Frédéric Vogel. Catalysis in supercritical water: Pathway of the methanation reaction and sulfur poisoning over a Ru/C catalyst during the reforming of biomolecules. *Journal of Catalysis*, 301(0):38 – 45, 2013.
- [39] Yin-Jia Zhang, Vijay Sethuraman, Ronald Michalsky, and Andrew A Peterson. Competition between CO₂ reduction and H₂ evolution on transition-metal electrocatalysts. *ACS Catalysis*, 4:3742–3748, 2014.
- [40] Youn-Geun Kim, Jack Hess Baricuatro, Alnald Javier, John Mathew Gregoire, and Manuel P Soriaga. The evolution of the polycrystalline copper surface, first to Cu (111) and then to Cu (100), at a fixed CO₂RR potential: A study by operando EC-STM. *Langmuir*, 2014.
- [41] S. Johnson and R.J. Madix. Sulfur induced selectivity changes for methanol decomposition on Ni(100). *Surface Science*, 103(2-3):361 – 396, 1981.

- [42] R. J. Madix, S. B. Lee, and M. Thornburg. The effects of adsorbed sulfur on the adsorption and reaction of CO and methanol on Ni(100). *Journal of Vacuum Science Technology A: Vacuum, Surfaces, and Films*, 1(2):1254–1260, apr 1983.
- [43] Adam C. Lausche, Frank Abild-Pedersen, Robert J. Madix, Jens K. Nørskov, and Felix Studt. Analysis of sulfur-induced selectivity changes for anhydrous methanol dehydrogenation on Ni(100) surfaces. *Surface Science*, (0):58–62, 2013.
- [44] Martin Winter and Ralph J Brodd. What are batteries, fuel cells, and supercapacitors? *Chemical reviews*, 104(10):4245–4270, 2004.
- [45] GA Camara, EA Ticianelli, S Mukerjee, SJ Lee, and J McBreen. The CO poisoning mechanism of the hydrogen oxidation reaction in proton exchange membrane fuel cells. *Journal of The Electrochemical Society*, 149(6):A748–A753, 2002.
- [46] JJ Baschuk and Xianguo Li. Carbon monoxide poisoning of proton exchange membrane fuel cells. *International Journal of Energy Research*, 25(8):695–713, 2001.
- [47] M Götz and H Wendt. Binary and ternary anode catalyst formulations including the elements W, Sn and Mo for PEMFCs operated on methanol or reformat gas. *Electrochimica Acta*, 43(24):3637–3644, 1998.
- [48] Lijun Yang, Shujuan Jiang, Yu Zhao, Lei Zhu, Sheng Chen, Xizhang Wang, Qiang Wu, Jing Ma, Yanwen Ma, and Zheng Hu. Boron-doped carbon nanotubes as metal-free electrocatalysts for the oxygen reduction reaction. *Angewandte Chemie*, 123(31):7270–7273, 2011.
- [49] H-F Oetjen, VM Schmidt, U Stimming, and F Trila. Performance data of a proton exchange membrane fuel cell using H₂/CO as fuel gas. *Journal of the Electrochemical Society*, 143(12):3838–3842, 1996.
- [50] S.R. Bahn and K.W. Jacobsen. An object-oriented scripting interface to a legacy electronic structure code. *Computing in Science Engineering*, 4(3):56–66, May/Jun 2002.

- [51] The DACAPO plane wave/pseudopotential DFT code is available as open source software at <http://www.fysik.dtu.dk/CAMPOS/>.
- [52] B. Hammer, L. B. Hansen, and J. K. Nørskov. Improved adsorption energetics within density-functional theory using revised Perdew-Burke-Ernzerhof functionals. *Physical Review B*, 59:7413–7421, Mar 1999.
- [53] David Vanderbilt. Soft self-consistent pseudopotentials in a generalized eigenvalue formalism. *Physical Review B*, 41(11):7892–7895, Apr 1990.
- [54] Alejandro Martinez-Ruiz, Ma.Guadalupe Moreno, and Noboru Takeuchi. First principles calculations of the electronic properties of bulk Cu_2O , clean and doped with Ag, Ni, and Zn. *Solid State Sciences*, 5(2):291 – 295, 2003.
- [55] Aloysius Soon, Mira Todorova, Bernard Delley, and Catherine Stampfl. Thermodynamic stability and structure of copper oxide surfaces: A first-principles investigation. *Physical Review B*, 75:125420, Mar 2007.
- [56] A. Kirfel and K. Eichhorn. Accurate structure analysis with synchrotron radiation. The electron density in Al_2O_3 and Cu_2O . *Acta Crystallographica Section A*, 46(4):271–284, Apr 1990.
- [57] A. Werner and H. D. Hochheimer. High-pressure x-ray study of Cu_2O and Ag_2O . *Phys. Rev. B*, 25:5929–5934, May 1982.
- [58] Tadasu Suzuki. X-ray study on the binding properties of Cu_2O and Ag_2O crystals. *Journal of the Physical Society of Japan*, 15(11):2018–2024, 1960.
- [59] Jens Kehlet Nørskov, Jan Rossmeisl, Ashildur Logadottir, Lars Lindqvist, John R Kitchin, Thomas Bligaard, and Hannes Jonsson. Origin of the overpotential for oxygen reduction at a fuel-cell cathode. *The Journal of Physical Chemistry B*, 108(46):17886–17892, 2004.

- [60] Andrew A. Peterson. Global optimization of adsorbate–surface structures while preserving molecular identity. *Topics in Catalysis*, 57(1-4):40–53, 2014.
- [61] Andrew A. Peterson, Lars C. Grabow, Thomas P. Brennan, Bonggeun Shong, Chinchun Ooi, Di M. Wu, Christina W. Li, Amit Kushwaha, Andrew J. Medford, Felix Mbuga, Lin Li, and Jens K. Nørskov. Finite-size effects in O and CO adsorption for the late transition metals. *Topics in Catalysis*, 55:1276–1282, 2012.
- [62] Ghazaleh Ghadimkhani, Norma R. de Tacconi, Wilaiwan Chanmanee, Csaba Janaky, and Krishnan Rajeshwar. Efficient solar photoelectrosynthesis of methanol from carbon dioxide using hybrid CuO-Cu₂O semiconductor nanorod arrays. *Chemical Communications*, 49:1297–1299, 2013.
- [63] Flemming Besenbacher and Jens K. Nørskov. Oxygen chemisorption on metal surfaces: General trends for Cu, Ni and Ag. *Progress in Surface Science*, 44(1):5 – 66, 1993.
- [64] Y. Hori, H. Wakebe, T. Tsukamoto, and O. Koga. Adsorption of CO accompanied with simultaneous charge transfer on copper single crystal electrodes related with electrochemical reduction of CO₂ to hydrocarbons. *Surface Science*, 335:258 – 263, 1995. Proceedings of the IUVESTA Workshop on Surface Science and Electrochemistry.
- [65] Hiroyuki Kato, Maki Kawai, and Jun Yoshinobu. Switching in the molecular orientation ruled by steric repulsion of adsorbed CO on Pd(110). *Physical Review Letters*, 82:1899–1902, Mar 1999.
- [66] P. Uvdal, P.-A. Karlsson, C. Nyberg, S. Andersson, and N.V. Richardson. On the structure of dense CO overlayers. *Surface Science*, 202:167 – 182, 1988.
- [67] Ellen D. Williams and W.H. Weinberg. The geometric structure of carbon monoxide chemisorbed on the ruthenium (001) surface at low temperatures. *Surface Science*, 82(1):93 – 101, 1979.

- [68] Waqar Ahmad, Musa Kaleem Baloach, and M Parvez. Computer simulation of the NO-CO reaction introducing CO-CO repulsion on a catalytic surface. *Chinese Journal of Physics*, 44(6):440–453, 2006.
- [69] Chuan Shi, Heine A. Hansen, Adam C. Lausche, and Jens K. Nørskov. Trends in electrochemical CO₂ reduction activity for open and close-packed metal surfaces. *Phys. Chem. Chem. Phys.*, 16:4720–4727, 2014.
- [70] Heine A. Hansen, Joseph H. Montoya, Yin-Jia Zhang, Chuan Shi, Andrew A. Peterson, and Jens K. Nørskov. Electroreduction of methanediol on copper. *Catalysis Letters*, 143(7):631–635, 2013.
- [71] C. Clay, S. Haq, and A. Hodgson. Hydrogen bonding in mixed OH+H₂O overlayers on Pt(111). *Physical Review Letters*, 92:046102, Jan 2004.
- [72] Joel Bernstein, Raymond E. Davis, Liat Shimoni, and Ning-Leh Chang. Patterns in hydrogen bonding: Functionality and graph set analysis in crystals. *Angewandte Chemie International Edition in English*, 34(15):1555–1573, 1995.
- [73] Paola Gilli, Valerio Bertolasi, Valeria Ferretti, and Gastone Gilli. Evidence for resonance-assisted hydrogen bonding. 4. Covalent nature of the strong homonuclear hydrogen bond. Study of the O-H-O system by crystal structure correlation methods. *Journal of the American Chemical Society*, 116(3):909–915, 1994.
- [74] Matthew Forster, Rasmita Raval, Javier Carrasco, Angelos Michaelides, and Andrew Hodgson. Water-hydroxyl phases on an open metal surface: breaking the ice rules. *Chemical Science*, 3:93–102, 2012.
- [75] F. Abild-Pedersen, J. Greeley, F. Studt, J. Rossmeisl, T. R. Munter, P. G. Moses, E. Skúlason, T. Bligaard, and J. K. Nørskov. Scaling properties of adsorption energies for hydrogen-containing molecules on transition-metal surfaces. *Physical Review Letters*, 99:016105, Jul 2007.

- [76] Kendra P Kuhl, Toru Hatsukade, Etosha R Cave, David N Abram, Jakob Kibsgaard, and Thomas F Jaramillo. Electrocatalytic conversion of carbon dioxide to methane and methanol on transition metal surfaces. *Journal of the American Chemical Society*, 136(40):14107–14113, 2014.
- [77] Manuela Bevilacqua, Jonathan Filippi, Alessandro Lavacchi, Andrea Marchionni, Hamish A Miller, Werner Oberhauser, Erik Vesselli, and Francesco Vizza. Energy savings in the conversion of CO₂ to fuels using an electrolytic device. *Energy Technology*, 2(6):522–525, 2014.